Mechanics and Mechanical Engineering
Vol. 16, No. 1 (2012) 51–71

Surface Vortices and Pressures in Suction Intakes of Vertical Axial–Flow Pumps

Andrzej Błaszczyk
Adam Papierski
Radosaw Kunicki
Mariusz Susik
Institute of Turbomachinery
Technical University of Łódź
andrzej.blaszczyk@p.lodz.pl
adam.papierski@p.lodz.pl
mariusz.susik@p.lodz.pl

Received (13 October 2012)
Revised (15 December 2012)
Accepted (5 January 2013)

In the article, there are introduced results of numerical computations of unsteady flow in the intake of large vertical pumps verified by results of the measurements made on the test stand.

Comparative analysis ofresults ofnumerical computations,pressuremeasurements and the observation of surface vortices, have confirmed the justness of a chosen computational method.

Keywords: Pump, inlet channel, cooling water system.

1. Introduction

Due to the increased demand for electrical and thermal power there are new power units being built in Poland, as well as currently working being modernized.

New huge power units and these being upgradedin terms of theincreased power, both require large supplies of the cooling water to the turbine condenser.

Most often there are mixed flow or axial flow pumps in the vertical system built into cooling water systems.

Due to the vertical construction of cooling water pumps, in their intake area, the flowing in water must change its' direction from horizontal to vertical. Change of the flow direction of huge amounts of water, inintake channels, is the existence cause of hydraulic phenomena which could disrupt or even stop the work of pumps. Changing theflow directionfrom horizontal toverticalis implementedin formed suction intakes, into whichthe water is drawn from wet wells.

The flow and hydraulic phenomena which take place in open wet wells play a major role in supplyinga liquidto thepumpimpeller.

Suction intake and outlet are final elements of the water intake system in pumps.

Scheme of theanalyzed real facility with marked elements of the pump intake system andits chosen geometrical parameters of the facility shown in the Fig. 1

The real pumping station facility (Fig. 1) consists of: the screen chamber (1), where are trash screens (2) used to roughlypurifythe water supply flowing in from thehigh–water source, (3) the rotary screen which task is to thorough purify the water from apollution, (4) the open wet well, (5) theformed suction intake and (6) the place for the cooling water pump installation.

In case of the wrong design of the formed suction intake and the open wet well, the flow can be characterized with typical of the unsteady flow:

- subsurface vortices (formed suction intake),
- surface vortices (open wet well),
- non–uniform distribution ofthe absolutevelocity axialcomponent in the impeller eye (suction chamber),
- liquid vortices in front of the impeller eye (suction chamber).

2. The open wet well

Wet well along with the built–in rotary screen covers an areacontainedbetween the outlet ofthe wet welland theformed suction intake. Wet well is an essential element of inflow channels supplying liquid to the axial flow pumps or mixed flow with the vertical axis, because of the water level, flow and geometry have the influence on the liquid inflowcharacterto the formed suction intake by controlling over thestructure ofthe flowin theinlet areaof a pump (Fig. 1).

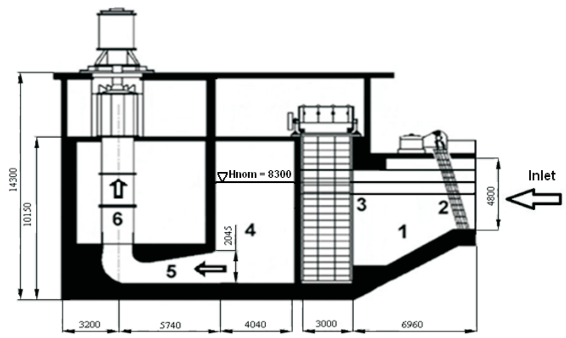

Figure 1 The real facility – system of the open wet well

The integral element of the wet well is a construction of the rotary screen, which also has an essential impact on the occurring inside hydraulic phenomena.

Vorticesarisingat the wet wellsurface, subsurfaceandbottomcan moveto the area ofthe pump inlet, causing anon–uniformflow ofthe liquidto theimpeller.

A particularthreat tothe pumparesurfacevortices, which can cause anaeration of thepumpand, consequently, adrop of the efficiency to zeroanddamagetothe machine.

Surface vortex is a phenomena arising at the water surface in open wet wells. It is caused by a non–uniform velocity distribution in the intake [14].

It arises in the case of differences in the flowvelocity in specific points of the wet well. If these differences are large, therefore at the water surface wondering vortices arise, which can cause a air suction to the pump, as it was stated above. Phenomena is the more intense the less is the level difference between the free surface of the liquid and the edge of theformed suction intake.

Based onmany years of experience, there wasdeveloped theclassification ofvortices[1], shownin Fig. 2.

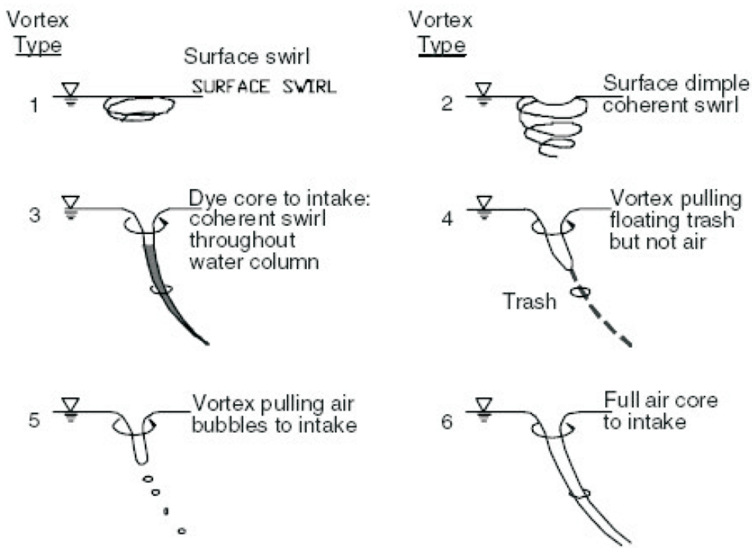

Figure 2 Classification of free surface vortices [1]

Based on observations ofthe free surface of liquid, it was found thatvorticeswhich occurin the class 1and 2 do not affect the operation of pumps. Vortices of the 3, 4, 5, 6 class are harmful and shouldbeeliminated [1].

In order to reduce and even eliminate surface vortices inwet wells of large centrifugal pumps, there have been carried out studies over the examination of the flow structure, by specialized laboratories TU Delft Hydraulic and CERG Grenoble in Europe, usingnumericalmethods forfluid dynamicsand theexperimentalvalidation [5, 6, 9, 10, 11, 12, 13].

Due to costs of experimental studies over the models of real facilities, large global and European experimental centers, in particular American, are tending to use only results of the numerical research in design procedures [5, 6, 9, 10, 11, 12, 13].

These publicationsrelate to intakeswith integratedinlet bells. Presented in articles results of numerical computations relate to the steady flow and differ from results of the liquid flow observation in models of intakes on test stands [9].

In the own research[3, 4] and thepublication [5] authorspoint to theneed fornumerical computationofthe flow,taking into account unsteady phenomena, which results should be validated using measurements and the experimental observation. In the article there is introduced a research of the numerical unsteady flow for the two construction variants of the suction intake model, made in a 1:10 scale in relation to the real facility (Fig. 1). Construction variants were introduced in the Fig. 8 and Fig. 9.

3. Numerical research of the unsteady flow in the intake

3.1. *Introduction*

Turbulent flow of the viscous, incompressible liquid is described by the Navier–Stokes equations, which along with the continuity equation constitute a complete dependence system allowing the determination of the pressure and flow velocity field. Time–averaged system was elaborated by Reynolds and constitutes the basic fluid mechanics formulas [2, 7]. N–S equation takes the form:

$$\frac{\partial(\rho U_i)}{\partial t} + \frac{\partial(\rho U_j U_i)}{\partial x_i} = -\frac{\partial P}{\partial x_i} - \frac{\partial}{\partial x_j}\tau_{ij} + \rho g \tag{1}$$

where:

ρ – density of a medium,
t – time,
g – gravitational acceleration,
U_j, U_i – momentary values of the velocity,
P – momentary value of the pressure,
x_i, x_j – geometric coordinates,
τ_{ij} – viscous stresses tensor.

Whereas the continuity equation takes the form:

$$\frac{\partial U_i}{\partial x_i} = 0 \tag{2}$$

$$U_i = \overline{U_i} + u_i \tag{3}$$

where:

U_i – momentary velocity value,
$\overline{U_i}$ – average velocity value,
u_i – value of the velocity fluctuation.

Graphical illustration of the Eq. (3) is shown in the Fig. 3.

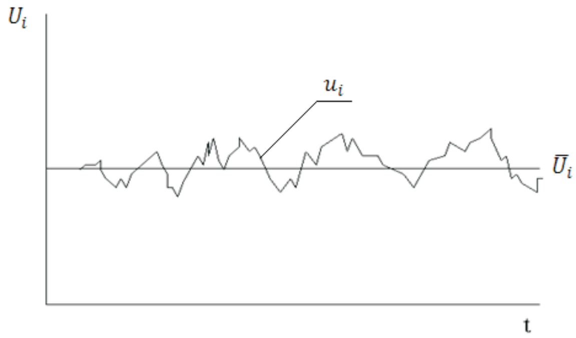

Figure 3 Momentary function of the velocity in time [6]

After taking into account that the momentary velocity can be described by the following dependence [2, 7]:

$$\overline{U_i} = \frac{1}{\Delta t}\int_t^{t+\Delta t} U_i dt \tag{4}$$

there is obtained the time–averaged continuity Eq. (5) using the Reynolds method (RANS) and the N–S equation for the incompressible fluid (6):

$$\frac{\partial \overline{U_i}}{\partial x_i} = 0 \tag{5}$$

$$\frac{\partial(\rho\overline{U_i})}{\partial t} + \frac{\partial(\rho\overline{U_j}\overline{U_i})}{\partial x_i} = -\frac{\partial\overline{P}}{\partial x_i} - \frac{\partial}{\partial x_j}(\overline{\tau_{ij}} + \rho\overline{u_i u_j}) + \rho g \tag{6}$$

where:
$\frac{\partial(\rho\overline{U_i})}{\partial t}$ – time term,
$\frac{\partial(\rho\overline{U_j}\overline{U_i})}{\partial x_i}$ – convection term,
$-\frac{\partial\overline{P}}{\partial x_i}$ – pressure term,
$-\frac{\partial}{\partial x_j}(\overline{\tau_{ij}} + \rho\overline{u_i u_j})$ – diffusion term,
ρg – mass forces term (taking into account the earthpull).
Quantity $\rho\overline{u_i u_j}$ is called the Reynolds strasses tensor and denoted as:

$$\overline{\tau_{ij}} = -\rho\overline{u_i u_j} \tag{7}$$

Stresses tensor requires modeling in order to close the (N–S) time–averaged equation using the turbulence model. For computations there was adopted the SST turbulence model.

3.2. *Method and boundary conditions of numerical computations*

Numerical computations of the flow have been carried out under the scheme elaborated by authors of the article shownin the Fig. 4.

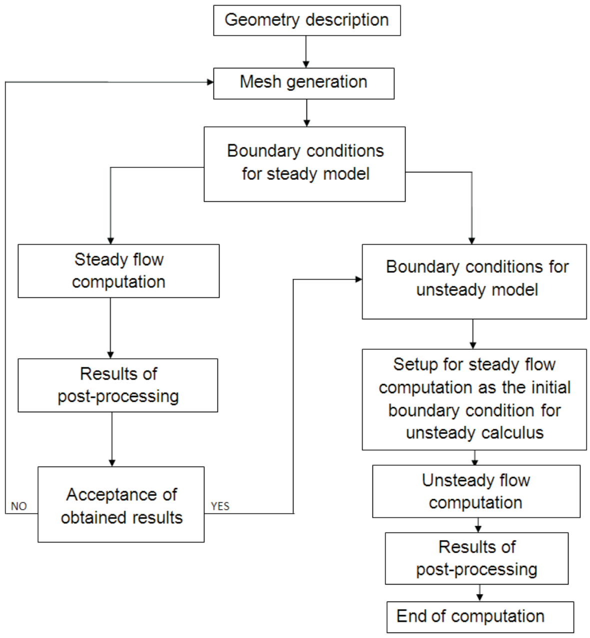

Figure 4 Scheme of the computation method of the unsteady flows [8]

Numerical computations under the scheme (Fig. 4) required the adoption of:

- the turbulence model,
- boundary conditions

On the basis of assumptions from the comparative analysis and a result of the initial numerical computation, the SST turbulence model has been adopted.

The SST turbulence model proposed by Menter, takes into account the transportation of the turbulent shear stresses in the SST model. In the SST model, the adequate representation of the turbulent stresses transportation was obtained by using the limiter in formulation of the turbulent viscosity [2, 7].

$$\mu = \frac{\rho\, a_1 k}{\max(a_1\,\omega, SF)} \tag{8}$$

where:

a_1 = 0,31,
k – kinetic turbulence energy,
ω – turbulence frequency,
F – transition function,
S – tensor invariant of the deformation velocity tensor.

In the adopted method, the transition function plays a major role. It is based on the distance value from the closest wall y and the flow parameters [2, 7].

$$F = \tanh\left[\max\left(\frac{2\sqrt{k}}{\beta'\,\omega\,y}, \frac{500\,\mu_t}{y^2\omega\,\rho}\right)\right]^2 \tag{9}$$

where:

k – kinetic turbulence energy,

ω – turbulence frequency,

μ_t – turbulence viscosity,

y – value of the distance to the closest wall.

Numerical calculus under the scheme (Fig. 4) requiresan assumption of boundary conditions, common for steady and unsteady computations:

- the total pressurein the inlet wet well definedby a formula (10).

$$p_c = \rho\,gH + \frac{\rho(Q/A_1)}{2} \tag{10}$$

where:

H – height of the water column in the wet well

ρ – water density

A – surface area of the connector of the screen chamberand the inlet of the wet well

Q – volume flow rate.

- a condition for the free surface generation according to the Fig. 5.

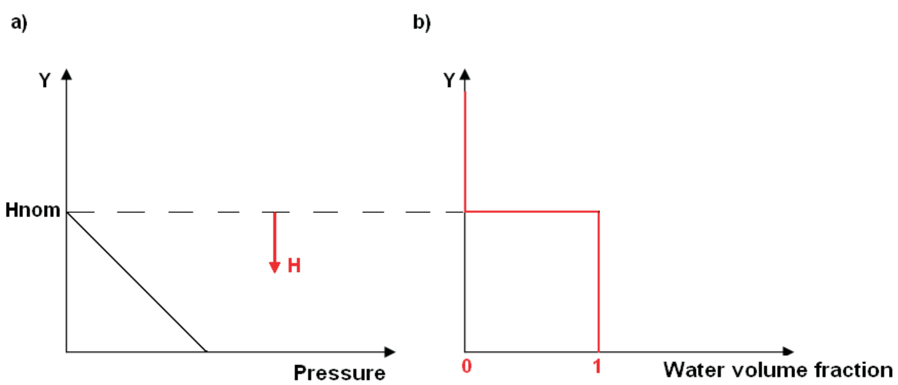

Figure 5 Boundary conditions of the inlet in the computational area of the inlet chamber: a) hydrostatic pressure b) water volume fraction

- the turbulence intensity at the level of 5 % (when $I = 10$) according to a formula:

$$I = \frac{\mu_t}{\mu_d} \tag{11}$$

where: μ_t – turbulent viscosity, μ_d – dynamic viscosity

- mass flow of the outflow pipe: $m = 24,6$ [kg/s],
- the zero gradient of the pressure in the direction of the main flow (this condition is assumed internally by the preprocessor of the ANSYS-CFX)

Unsteady conditions require additional settings:

- work area of the rotary screen to the total area of the screen is 74%
- assumed loss of pressure at the screen $\Delta p = 60$ Pa,
- quadratic resistance coefficient:

$$K_Q = \left(\frac{\Delta p}{\Delta x}\right) c_{por}^2 \tag{12}$$

where:

Δp – pressure loss at the porous surface

Δx – thickness of the screen (porous surface)

c_{por} – flow velocity of the liquid through the porous surface

- hydraulically smooth walls have been assumed,
- a logarithmicvelocity distributionon the wall has beenassumed – the so–called wall function.

In the Fig. 6 below has been shown the diagram of dimensionless velocity $u+$ in the function of dimensionless distance from the wall $y+$. To have the wall function working correctly, the first mesh node has to lie in the distance not smaller than $y+ = 12$ and not further than $y+$=200 (Fig. 7). For the value $y+$ <11 the mesh node lies in the laminar sub–layer and for $y+$ >300, beyond the boundary layer.

- a Courant number – is the basic criterion of the unsteady flow calculus defined as:

$$\text{Courant} = \frac{u\,\Delta t}{\Delta x} \tag{13}$$

where:

u – the average velocity,

Δt – the time step,

Δx – the size of the mesh cell.

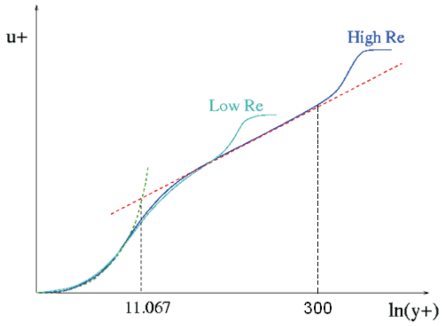

Figure 6 The range of values $y+$ [2]

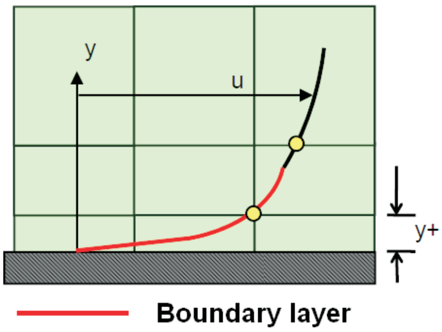

Figure 7 The position of the first mesh node in the boundary layer in the area of logarithmic velocity distribution (boundary layer) [2]

The scope of Courant number values, for the numerical computations, using the turbulence model SST, is not formulated. It is advisable to take such value, which allows for obtaining solution with the assumed level of convergence [2]. In consideredmodels ofthe wet wellandthe formed suction intake, the value of Courant number is ranged in the scope (0.082.04) and for this value there was obtained the assumed level of convergence,

- the total time of computations: 30 [s],
- the time step: 0.001 [s],
- the minimal number of iterations for the given time step: 1,
- the maximal number of iterations for the given time step: 12,
- discretisation degree of the convective term: II order,
- the solution recording time step: 0.05 [s],

- tetrahedral mesh used in numerical computations,
- amount of control volumes in the case of the intake with barriers equals to 2,4 mln, without barriers equals to $\approx$ 1,6 mln
- number of the mesh nodes for the intake with and without barriers equals to $\approx$ 1 mln.

Geometry and the computation mesh for the intake with barriers is shown in the Fig. 8 (variant 1). and for the intake without barriers in the Fig. 9 (variant 2).

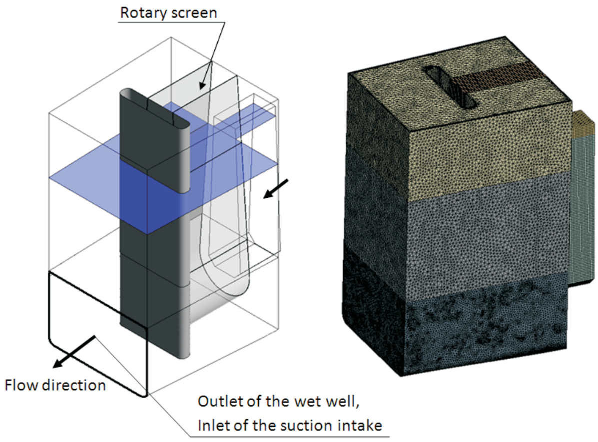

Figure 8 Geometry and computation mesh for the model of the intake without barriers. Variant 1

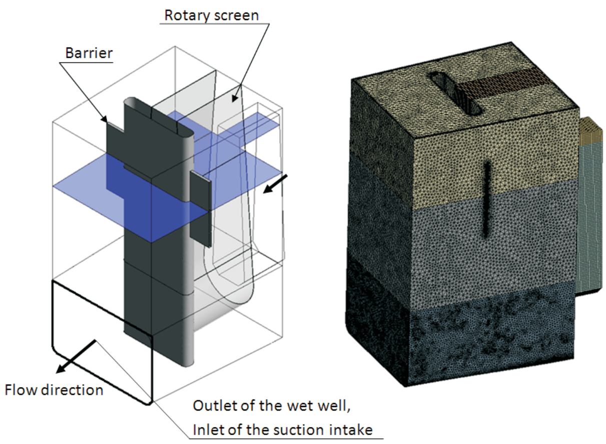

Figure 9 Geometry and computation mesh for the model of the intake with barriers. Variant 2

The analysis of obtained results of the unsteady computations quality consisted of checking the level of unbalanced mass flows and momentum in the control volumes of the mesh – a so called residuum [2] (it determines the qualityof obtained results), which for the each of the results was in the range of. This level informs that the solution has a good convergence and which results will be validated with observations taking place on the test stand.

3.3. *A plan of the numerical calculus*

Numerical computations of flow local parameters for the two construction variants, were carried out for the nominal liquid level in the intake of the facility (Fig. 1, $(H_{nom})_m = 8,3$ m and $(Q_{nom})_m = 28050$ m^3/h).

Numerical computations validations were realized by results of flow measurements and observations on the test stand (chapter 4).

In the research of the model on the test stand, these values were corresponded with following values: $(H_{nom})_m = 0,665$ m and $(Q_{nom})_m = 88,702$ m^3/h

Dimensionedvariant ofthe intakewith marked direction of the flow, measurement points of the pressure at the bottom of the wet well, curtain walls and the grid with threads shown in the Fig. 10.

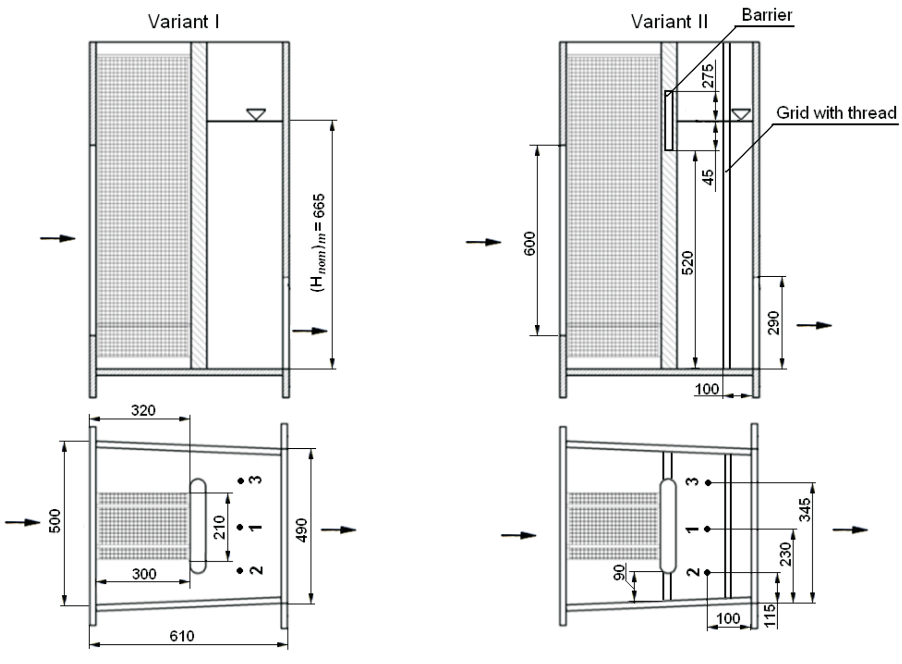

Figure 10 Model of the intake Variant 1 without the barrier, variant 2 with the barrier

Barriers (variant 2) were introduced after computations and research of the variant 1. Barriers in the chamber were placed for the flow visualization in the neighborhood of the suction intake. On the bottom of the intake were made measurement holes in order to measure pressures.

4. The test stand

4.1. *Construction of the stand*

The test stand enabled carrying out measurements and observations of values computed numerically.

Geometrical and flow parameters of the model were determined on the basis of the Froude (Fr) numbers equality condition for the facility and the model $Fr_o = 1.094 \approx Fr_m = 1.093$. Because the Reynolds' number $Re > 3 *10^4$ and the Weber number $We > 120$, far outweigh the critical values, it can be stated that the dynamic similarity condition between the object and the model is satisfied.

The test stand is shown in the Fig.11.

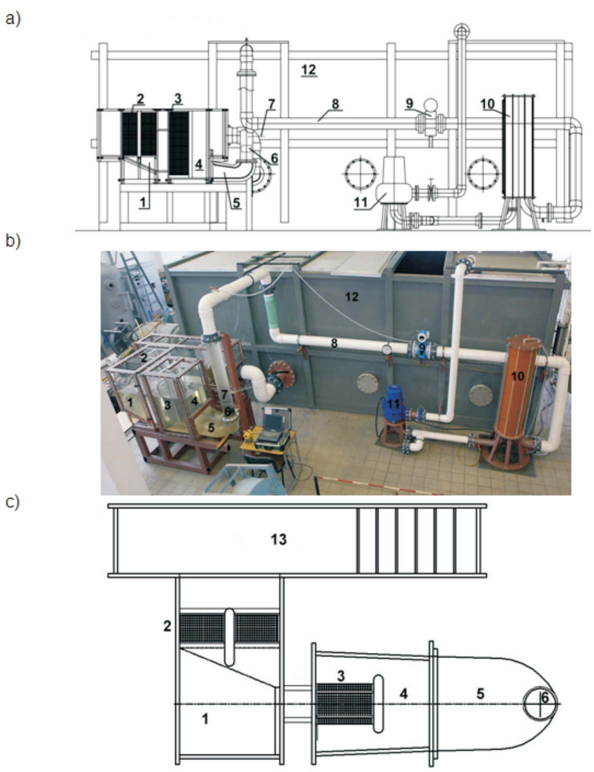

Figure 11 The test stand [3, 4] a)elevation of the test stand, b) view of the test stand, c) system of the wet well (top view)

The test stand consists of: the screen chamber (1), inlet screens (2), the rotary screen (3), the wet well (4), the formed suction intake (5), the swirl meter (6), the Pitot probe (7), pipelines (8), theflowmeter (9), the steam–waterseparation tank (10), the circulating pump (11), the main water tank (12), the delivery channel – model of the high–water source (13)

For validation of numerical computation results in the intake, there were used results of the observation of surface vortices, threads attached togrid nodes andpressure measurements inpressure holesat the bottom of the wet well (Fig. 10) made during the realization of measurements, discussed in [3, 4].

Measures and recordings of the pressure were made with the differential transducer ofMobrey company – type 4301D2, with thepre–set measuring range -2500 ÷ +2500 Pa, with the guaranteed tolerance ±5 Pa. The view of the apparatus shown in the Fig. 12.

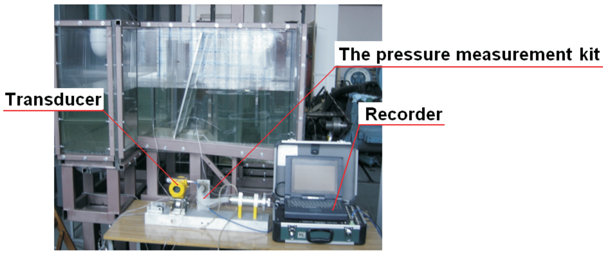

Figure 12 Kit for measuringthe pressureat the bottom ofthe wet well

5. The comparative analysis of computation results and measurements

5.1. *The pressure at the bottom of the suction intake*

System for pressure measurements was adapted for measuring changes with a time–constant of several seconds. Because of the unsteady nature of the flow in the intake, there were compared average values of pressures computed numerically.

In the Tab. 1 there is a comparison of pressure values obtained from the measurement for $(H_{nom})_m$ and $(Q_{nom})_m$ variant I.

Table 1

Pressures in the pressure holes at the bottom of the wet well for $(H_{nom})_m$ and $(Q_{nom})_m$, variant I - measurements		
hole 2	hole 1	hole 3
p [Pa]	p [Pa]	p [Pa]
6394,72±5	6399,44±5	6395,45±5

Measured pressures in pressure holes 1–2–3 in the variant II of the formedsuction intake were the same as in the variant I.

In the Tab. 2 are compared values of numerically computed values for each pressure hole in the variant I of the formedsuction intake.

Time–averaged values of pressures computed numerically for H_{nom}, Q_{nom} variant I

Table 2

Pressures in the pressure holes at the bottom of the wet well for $(H_{nom})_m$ and $(Q_{nom})_m$, variant I		
hole 2	hole 1	hole 3
p [Pa]	p [Pa]	p [Pa]
6402,67	6410,8	6401,63

In the Ttab. 3 there are shown the time–averaged pressure values computed numerically for the nominal parameters of the intake operation H_{nom}, Q_{nom}, variant 2.

Table 3

Numerically computed values of the pressure in measurement holes on the bottom of the wet well for $(H_{nom})_m$ and $(Q_{nom})_m$, variant 2		
hole 2	hole 1	hole 3
p [Pa]	p [Pa]	p [Pa]
6401.8	6406.23	6400.8

Runs of variables in time of computed pressures and their average values for each hole shown in the Fig. 13 and Fig. 14 adequate for the intake without barriers and with barriers.

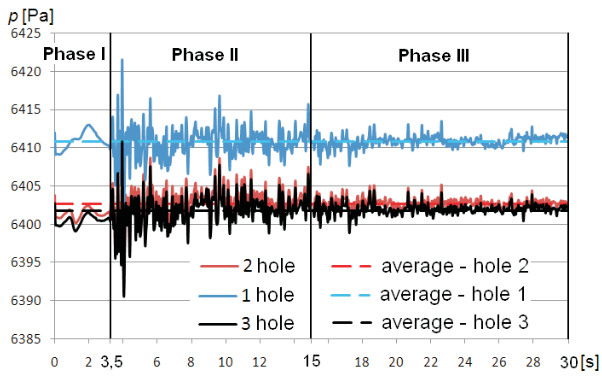

Figure 13 Characteristic values, temporary and mean in pressure holes 1 - 2 - 3 obtained in numerical computations. Variant 1

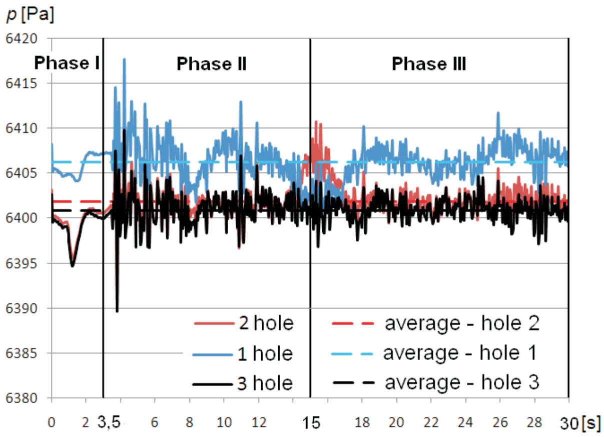

Figure 14 Characteristic values, temporary and mean in pressure holes 1 - 2 - 3 obtained in numerical computations. Variant 2

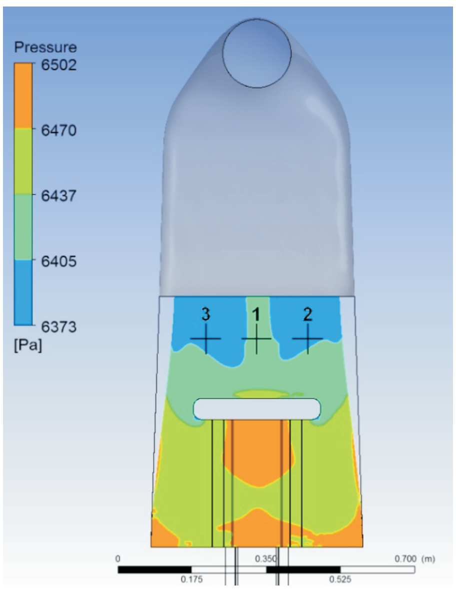

Figure 15 The distribution of numerically calculated pressures at the bottom of the formed suction intake for the variant 1 and 2

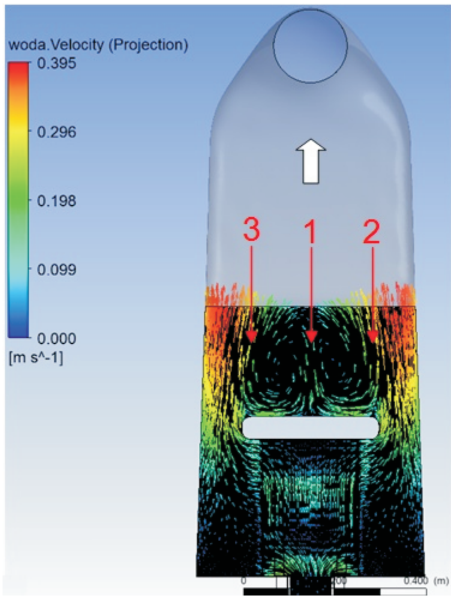

Figure 16 Velocity distribution in the neighborhood of points 1-2-3 of the pressure measurement for the variant 1 and 2

In Fig. 13 and Fig. 14 were also marked, with the vertical lines, boundaries of transient phases from the steady flow to the RANS flow.

Measured differences of pressures see Tab. 1 variant 1, Tab. 2 variant 2, confirmed using numerical computations Fig. 15.

Fig. 15 shows the equality of pressures in pressure holes "2" and "3". In relation to the pressure in the pressure hole 1, they characterize with the less value. The cause of smaller pressures are bigger values of the velocity in the neighborhood of "2" and "3' points, in relation to the velocity in the neighborhood of point 1 (Fig. 16).

Velocity distribution in the neighborhood of points 1–2–3 is confirmed by the pressure distribution from measurements and numerical computations. In the point 1 there occurs a velocity drop of both vortices in the neighborhood of this point.

5.2. *The flow visualization of vortices in the wet well.*

For work parameters of the wet well $(H_{nom})_m$ and $(Q_{nom})_m$ two variants of the chamber construction (Fig. 10) there were performed:

- numerical computations of fluid flow parameters, on the basis of which, visualizations were made,

- observations of the flow on the test stand, with use of the inhabited pointwise colorant and grids with threads installed in the wet well in the distance of 10 cm from the inlet to the formed suctionintake (Fig. 10).

In Figs 17, 18 ,19 there are shown graphic illustrations of the numerical computation and observations of the flow on the test stand.

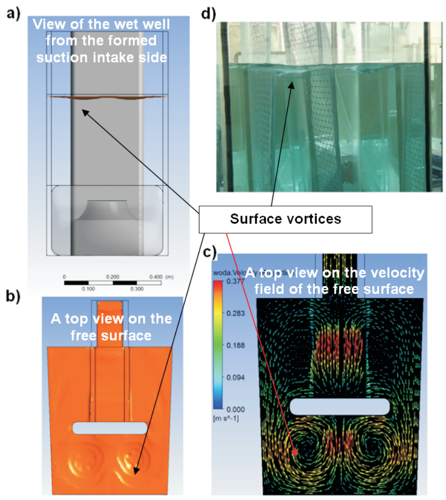

Figure 17 Surface vortices in the wet well. Variant 1 (without barriers) a), b), c) visualization of the flow based on numerical computations, d) observation of vortices on the test stand

During the flow through the wet well, there were noticed, appearing in the 30 sec intervals, momentary ($\approx$ 5 sec.) surface vortices without air bubbles under the water surface. A surface condition in the wet well meets a standard of 1–2 class due to the vortex classification Fig. 2.

Simultaneously, it can be confirmed the compatibility of the free surface of the liquid condition being a result of numerical computations and conditions observed on the test stand.

Due to the necessity of increase of the cooling water pump efficiency up to the value of $Q_{max} = 1.2\mathrm{Q}_{nom}$,for instance in the case of the water temperature increase or the momentary power increase in a power unit, there were also performed numerical computations of the flow for H_{nom} and Q_{max}. In the Fig. 18 were show free surfaces obtained as a result of numerical computations for H_{nom} and Q_{max} and observations made on the test stand.

During the flow there occur vortices of the class 3 in which dispersed air bubbles constantly reach the inlet to theformed suction intake.

In spite of the fact that the standard [1] does not allow the existence of the class 3 vortices at the free liquid surface in the wet well, curtain walls shown in the Fig. 10b. were used.

Graphic illustration of the free liquid surface condition determined on the basis of numerical computations and observations on the test stand, show in the Fig. 19.

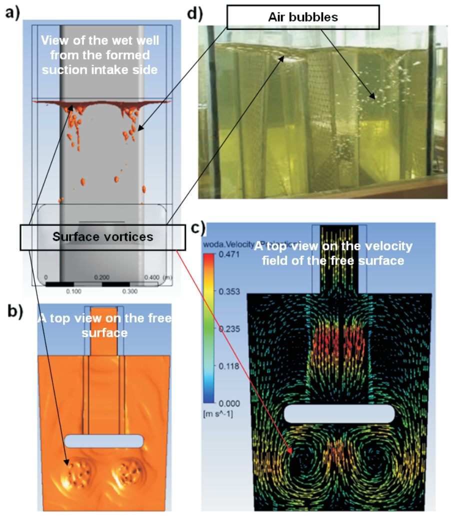

Figure 18 Surface vortices and air bubbles in the wet well.Variant 1 (without barriers). a), b), c) theflow visualization based on numerical computations results, d) observations of vortices and air bubbles on the test stand

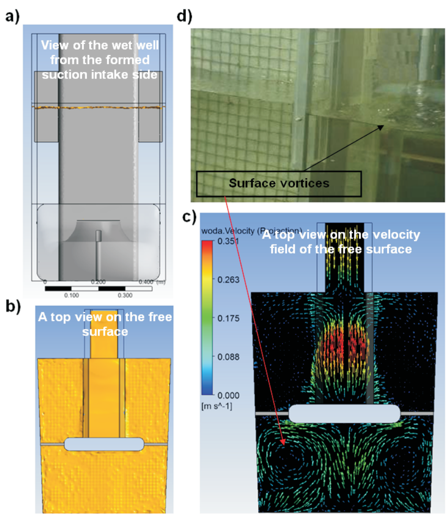

Figure 19 Surface vortices in the wet well. Variant 2 (with barriers). a), b), c) the flow visualization based on numerical computations, d) observations of vortices on the test stand

Presented condition of the free liquid surface fulfills requirements of the class 1 vortices. There were also performed visualizations of the flow in the neighborhood of the outlet to the inlet chamber. In the Fig. 20 is shown the numerically computed velocity distribution in the plane perpendicular to the direction of the flowin the distance of 10 cm from the suction chamber. In the neighborhood of the front wall and the inlet to the formed suction intake there was noticed a backward flow.

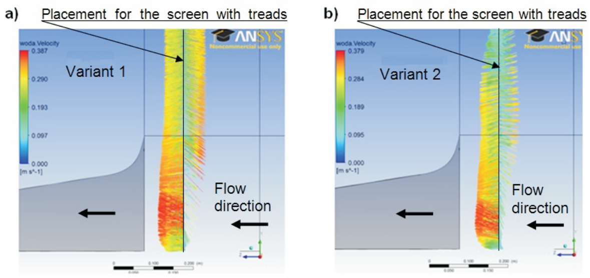

Figure 20 Velocity vectors distribution in the neighborhood of the inlet to the suction intake

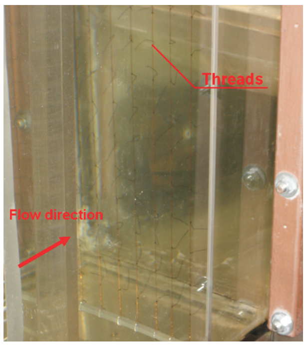

Figure 21 View of the grid with threads

Obtained numerical computation based distributions were confirmed by the observation of threads attached to the grid (Fig. 21).

6. Conclusions

Conclusions andfinal remarkscan berepresented as following points:

1. Changes, during numerically computedpressures, prove the unsteadynatureof the flow inthe wet well(Fig.13, Fig. 14),
2. Minimal differences between computed and measured mean pressures arise from:

- the pressure measurement uncertainty, includingthe dynamics ofthe measurement system,
- participation of the dynamic pressure in the value of measured pressure.

From the comparison of tables T-1 and T-2, T-1and T-3 it follows that for each pressure hole, the pressure is smaller than averaged pressures computed numerically.

From the Fig. 14 it follows the equality of pressures in pressure holes 2 and 3.

In relation tothepressurein the hole 1theyare characterized bylower values. A cause of less pressure values are larger velocities in the neighborhood of 2 and 3 points in relation to velocities in the neighborhood of point 1 (Fig. 16).

1. In the plot Fig. 13, Fig. 14 there can be distinguished three phases of the pressure change:
   - Phase 1. Change of the pressure is characteristic for the transition from the steady to RANS flow.
   - Phase 2. Initially pressures amplitudes dramatically increase and secondly randomly decrease.
   - Phase 3. In this phase fluctuation of the pressure are stabilizing what is characteristic of the RANS flow.
2. The condition of free surfaces in the wet well, based onnumerical computations, is similar to the free surface condition observed on the test stand (Fig. 17, 18, 19).
3. For nominal parameters of work of the intake $(H_{nom})_m$ and $(Q_{nom})_m$ the free surface condition meets the class $1-2$ according to the vortices classification in [1].
4. In the case of work parameters of the chamber $(H_{nom})_m$ and $(Q_{max})_m$, there occurred surface vortices and air bubbles constantly flowing into the formed suction intake. According to the vortices classification [1] these are vortices of the $3-4$ class.
5. Introduction of curtain walls caused a drop of vortices of the class 3 to the class 1.
6. The proposed numerical calculus algorithm may be used in the analysis of unsteady flows in pumpintakes.

References

[1] **American National Standard for Pump Intake Design**, ANSI/HI 9.8-1998. Hydraulic Institute. 9 Sylvan Way, Parsippany, New Jersey 07054-3802, www.pumps.org

[2] **ANSYS CFX**, Release 12.1: Theory Manual, **2001**.

[3] **Błaszczyk, A., Najdecki, S., Papierski, A., Staniszewski, J.**: Model examinations of the suction intake of the cooling water pump 180P19 on the test stand no. 8 for a unit A 460MW in Ptnów Power Plant, Report of the work stage I, *Archives of the Institute of Turbomachinery TU of Łódź*, 1542, **2006**.

[4] **Błaszczyk, A., Najdecki, S., Papierski, A. and Staniszewski, J.**: Model examinations of the suction intake of the cooling water pump 180P19 on the test stand no. 8 for a unit A 460MW in Ptnów Power Plant, Report of the work stage II, *Archives of the Institute of Turbomachinery TU of Łódź*, 1546, **2006**.

[5] **Karassik, I. J., Messina, J. P., Cooper, P. and Heald, Ch. C.**: Pump Handbook, Third Edition, *McGraw–Hill*, New York, **2001**.

[6] **Kazimierski, Z.** Numeryczne wyznaczenie trójwymiarowych przepływów turbulentnych, *Maszyny Przepływowe*, Wrocław, Vol. 11, **1992**.

[7] **Kuczkowski, M.**: Numeryczny model turbulencji przepływu przez zagięcie przewodu z wykorzystaniem metody LES, *Ph. D. thesis*, Łódź, **2007**.

[8] **Kunicki, R.**: Numeryczne i doświadczalne badania przepływów nieustalonych w komorach wlotowych pomp, *Ph. D. thesis*, Łódź, **2011**.

[9] **Li, S., Lai, Y., Weber, L., Silva, J.M. and Patel, V.C.**: Validation of a 3D Numerical Model for Water Pump Intakes, *Journal Hydraulic Research*, 42(3), 282–292, **2004**.

[10] **Mahesh, K., Constantinescu, S. G. and Moin P.**: A Numerical Method for Large Eddy Simulation in Complex Geometries, *Journal of Computational Physics*, 197(1), 215–240, **2004**.

[11] **Menter, F.R.**: Multiscale model of turbulent flows, *AIAA, 24^{th} Fluid Dynamic Conference*, **1993**.

[12] **Rajendran, V. P., Constantinescu, S. G. and Patel, V. C.**: Experimental Validation of Numerical Model of Flow in Pump–Intake Bays, *Journal of Hydraulic Engineering*, 125(11), 1119–1125, **1999**.

[13] **Tullis, J.P.**: Modeling in design of pumping pits, *Journal of the Hydraulic Division*, Vol. 105, No. HY9, P. 1053–1063, **1979**.

[14] **Zaino, A.**: Wpływ parametrów konstrukcyjnych na zjawiska przepływowe w komorach wlotowych zamkniętych dużych pomp wirowych, *Technical University of Wrocław*, **1994**.